Supplementary Materials

Anticipating Decoherence: a Predictive Framework for Enhancing Coherence in Quantum Emitters

Pranshu Maan[1,3,7], Yuheng Chen[1,3,7], Sean Borneman[1,2], Benjamin Lawrie[5], Alexander Puretzky[4], Hadiseh Alaeian[1,6,7], Alexandra Boltasseva[1,3,7], Vladimir M. Shalaev[1,3,6,7*], Alexander V. Kildishev[1,7*]

[1]Elmore Family School of Electrical and Computer Engineering, Birck Nanotechnology Center, Purdue University, West Lafayette, 47907, IN, USA.
[2]now at Carnegie Mellon University, 7325 Wean Hall, 5000 Forbes Ave, Pittsburgh, 15213, PA, USA.
[3]Quantum Science Center (QSC), Oak Ridge National Laboratory, Oak Ridge, 37830, TN, USA.
[4]Center for Nanophase Materials Sciences, Oak Ridge National Laboratory, Oak Ridge, 37830, TN, USA.
[5]Materials Science and Technology Division, Oak Ridge National Laboratory, Oak Ridge, 37830, TN, USA.
[6]Department of Physics and Astronomy, Birck Nanotechnology Center, Purdue University, West Lafayette, 47907, IN, USA.
[7] Purdue Quantum Science and Engineering Institute, Purdue University, West Lafayette, 47907, IN, USA.

*Corresponding author(s). E-mail(s): shalaev@purdue.edu; kildishev@purdue.edu;
Contributing authors: pmaan@purdue.edu, maan@umich.edu; chen4114@purdue.edu; sbornema@andrew.cmu.edu; lawriebj@ornl.gov; puretzkya@ornl.gov; halaeian@purdue.edu; aeb@purdue.edu;

Keywords: Anticipatory Systems, Solid State Quantum Optics, Coherence, Machine Learning, Artificial Intelligence

S1 Characterizing quantum emitters

The photoluminescence (PL) measurements were performed using a standard confocal optical setup. In this study, no polarization control or intensity calibration was applied; thus, the reported PL intensities are presented in arbitrary units. Polarization effects were not investigated. Additional information on these emitters is available in Refs.[1, 2], while studies on spectral diffusion across different platforms can be found in [3]. For further discussion on residual spectral diffusion despite feedback mechanisms, see [4].

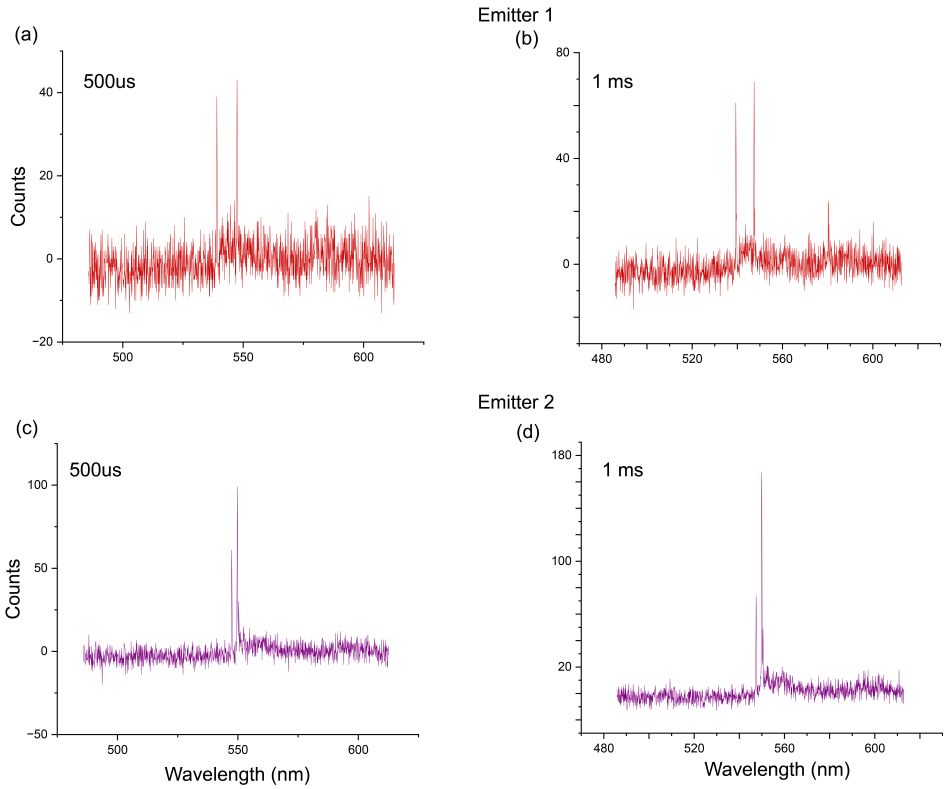

Fig. S1 Experimental characterization of spectral diffusion in SiN quantum emitters: (a) Quantum emitter spectra for Emitter 1, acquired at 500µs interval. (b) Acquired at 1ms; ZPL can be observed at 539.55nm for Emitter 1 and 550.76nm for Emitter 2. Si-Raman lines for both emitters are at 547.44nm (c) The quantum emitter spectra for Emitter 2, acquired at 500µs interval. (d) Acquired at 1ms.

S1.1 Individual emitter spectra

To obtain the time traces of both the zero-phonon line (ZPL) and the Si-Raman feature, emission spectra from both emitters with acquisition times of 500µs and 1ms were recorded using a 532nm excitation laser at approximately 1mW power (see *Methods*),

as shown in Fig. S1. The 500µs acquisition time is well suited, as spectral diffusion typically occurs on timescales ranging from sub-µs to several tens of ms. Acquisition of 1ms was included for comparison.

S1.2 Time evolution of ZPL

The input to the internal prediction model is the time trace of the ZPL acquired at 500µs acquisition rate. To accurately track the ZPL during spectral diffusion analysis, we imposed wavelength constraints tailored to each emitter. For Emitter 1, the tracked wavelength was restricted to a window spanning 10 nm below and 5 nm above 540 nm. This range effectively excludes the silicon Raman line at 547.44 nm, preventing its misidentification as the ZPL. Without such constraints, transient drops in ZPL intensity below the Raman peak could lead to erroneous peak assignments, introducing artificial discontinuities in the spectral trajectory. By limiting the analysis to a physically justified wavelength window, we ensure that the tracked peak faithfully represents the emitter's ZPL rather than unrelated spectral features. Similarly, for Emitter 8, the lower bound was set at 549 nm to exclude the Si-Raman line region, with an upper bound of 555 nm (5 nm above 550 nm) to avoid intermittent wavelength jumps. These targeted constraints maintain data integrity and enable robust tracking of spectral diffusion.Figure S2 represents the time trace of two emitters.

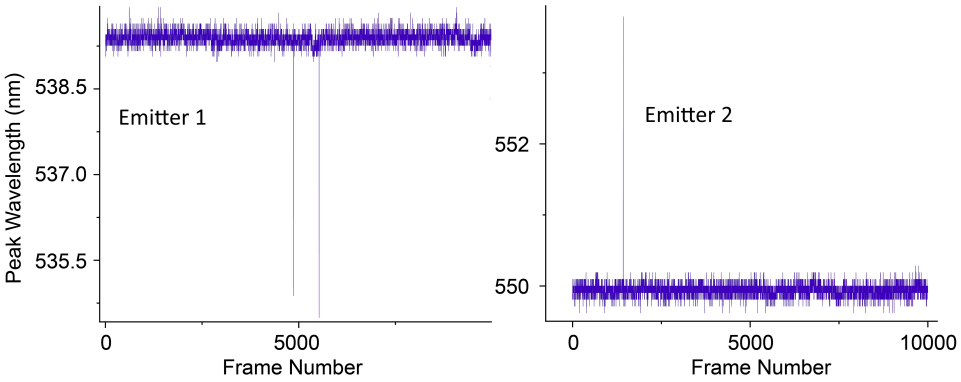

Fig. S2 Temporal evolution of zero-phonon line (ZPL) for two quantum emitters under non-resonant 532 nm excitation (≈ 1 mW): The x-axis represents the sequential frame number, where each frame corresponds to a single spectrum acquired with a 500 µs integration time. The y-axis indicates the ZPL peak wavelength tracked across the full time series. For each emitter, 10,000 consecutive spectra were recorded, enabling precise reconstruction of ZPL dynamics.

S1.3 Individual spectra for Power Spectral Density (PSD) estimation

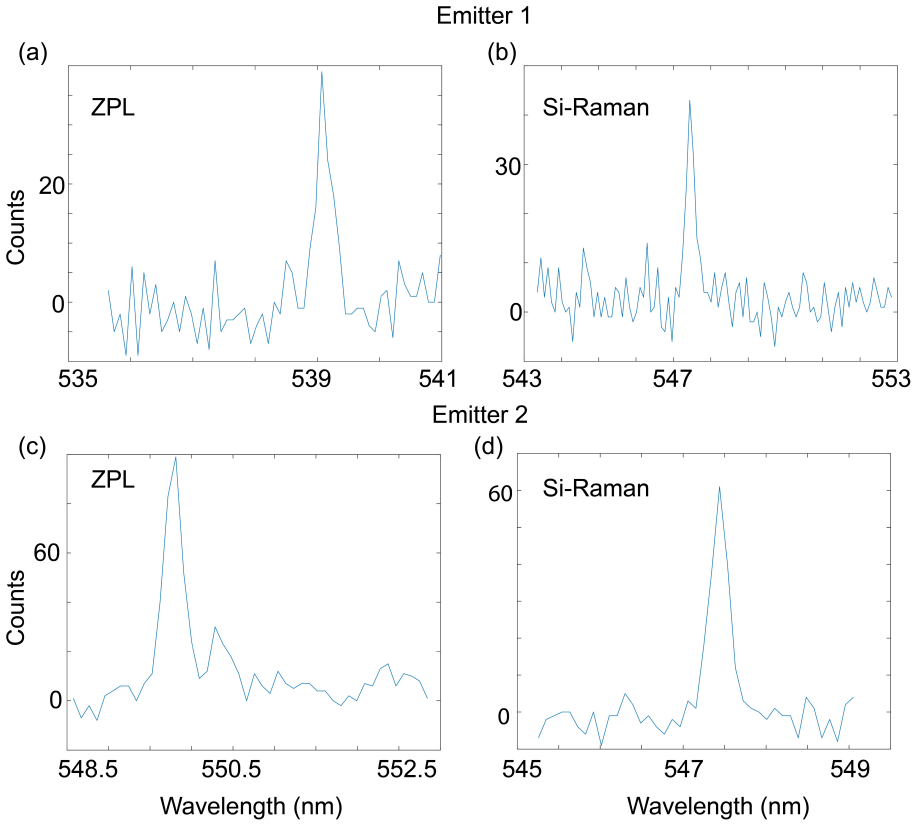

Fig. S3 Splitting ZPL and Si-Raman in emitter spectra for $1/f$ characterization: (a) Quantum emitter spectra for Emitter 1, acquired at 500µs interval showing ZPL at 539.55nm and 550.76nm for Emitter 2 in (c). Si-Raman lines for both the emitter is at 547.44nm as shown in (b) and (d).

For faithful tracking of the zero-phonon ZPL during PSD and ACF analysis, a specific portion of the spectrum containing the ZPL—illustrated in Figure S3—was extracted for each spectral sample. PSD and ACF calculations were then performed on this subset of data.

It appears that Emitter 2 in this study exhibits greater spectral instability, as evidenced by its larger deviations from the average spectral behavior, particularly visible in the temporal evolution of the order parameter (see Fig. 3(c) in the main manuscript). One possible explanation for this behavior is the emergence of a side peak near 550.5nm, as shown in Fig. S4, which may arise due to a nearby defect

or an adjacent quantum emitter. Variations in decoherence within the surrounding environment could be a contributing factor to this relative instability.

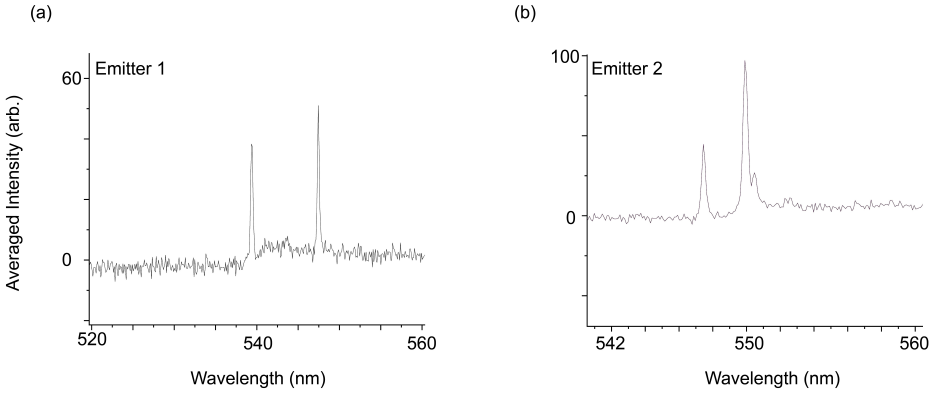

Fig. S4 Emitter-averaged spectra. (a) Quantum emitter averaged spectrum for Emitter 1, acquired at 500 µs intervals, showing a zero-phonon line (ZPL) at 539.55 nm. (b) Corresponding spectrum for Emitter 2, with a ZPL 550.76 nm. Both spectra also show a silicon Raman line at 547.44nm. Each spectrum was averaged over 10,000 samples. Notably, Emitter 2 displays a distinct side peak near 551 nm, which is unlikely to be noise and may indicate the presence of a nearby defect or a different emitter.

S2 Order parameter estimation

We present a statistical formalism for spectral diffusion grounded in replica theory (see *section 2.2* in the main manuscript), designed to characterize spectral dynamics relative to the emitter's ensemble-averaged response arising from interactions with its environment [5]. In contrast, Pearson correlation enables pairwise comparison between individual spectra but does not capture how each spectrum deviates from the global, averaged response of the emitter. As shown in Equation (S2), this framework is expressed in terms of an order (or overlap) parameter, $|q|$, which represents the normalized scalar product between spectral frames fluctuation from the average response. The parameter $|q|$ ranges from 0 to 1, where $|q| = 0$ indicates no overlap, and $|q| = 1$ indicates perfect overlap.

A spectral *sample* is defined as a set of 1340 wavelengths that form one PL spectra acquisition and their corresponding emission intensities, represented as a column vector $\mathbf{s} \in \mathbb{R}^{1340}$. A *dataset* refers to the complete collection of all samples acquired from a given emitter. Each dataset contains 10,000 such samples, i.e., PL spectra taken consecutively. A *frame* $\mathbf{F}$ is defined as a group of consecutive PL spectral samples, with the number of PL spectrum samples specified by the *frame size* ($fSize$). For instance, if $fSize = 50$, then each frame comprises 50 PL spectrum samples and is represented as a matrix $\mathbf{F} \in \mathbb{R}^{fSize \times 1340}$. The *frame step* is defined as $fStep \in [1, fSize]$ and it determines the sampling interval between frames. A minimum step ($fStep = 0$) corresponds to maximum overlap between successive frames, while a maximal step ($fStep = fSize$)

corresponds to zero overlap. In the zero-overlap case, the total number of frames is simply the total number of samples divided by frame size ($N = \frac{10{,}000}{fSize}$).

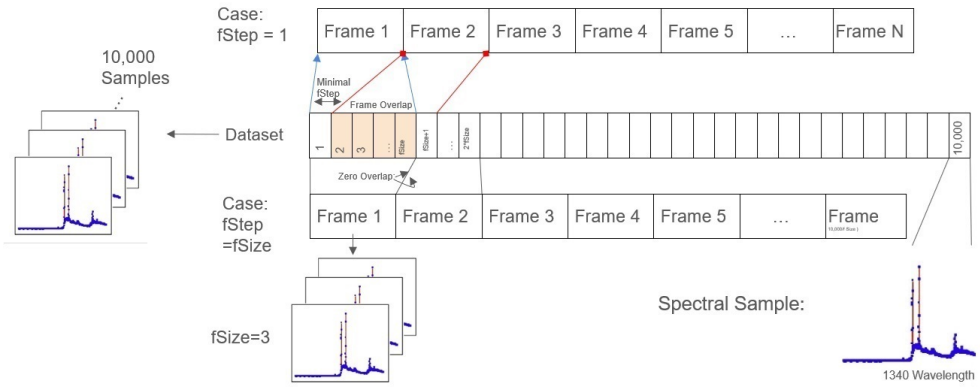

Fig. S5 Order parameter estimation data visualization: Each spectral sample comprises 1,340 discrete wavelength points acquired in a single spectrometer measurement. A complete dataset consists of 10,000 such spectral samples collected sequentially. For analysis, samples are grouped into frames, where the frame size (e.g.,fSize=3) denotes the number of consecutive spectral samples aggregated per frame. The frame step parameter (fStep) defines the offset between two consecutive frames: a minimal fStep introduces maximum overlap, whereas fStep = fSize corresponds to zero overlap between frames.

The dataset-averaged frame $\bar{\mathbf{F}}$ used in the order parameter calculation is computed by element-wise summation of all frames followed by normalization:

$$\bar{\mathbf{F}} = \frac{1}{N} \sum_{n=1}^{N} \mathbf{F}_n \tag{S1}$$

The order parameter matrix $\mathbf{q}$ is then constructed in two steps: first, we subtract the average frame from each frame to obtain the deviation $\mathbf{\Delta}_n = \mathbf{F}_n - \bar{\mathbf{F}}$; second, we compute each matrix element as the normalized scalar product between deviations:

$$q_{n,m} = \frac{\langle \mathbf{\Delta}_n, \mathbf{\Delta}_m \rangle}{\|\mathbf{\Delta}_n\| \, \|\mathbf{\Delta}_m\|} \tag{S2}$$

This results in a symmetric matrix $\mathbf{q} \in \mathbb{R}^{N \times N}$, where $q_{n,n} \equiv 1$ and $q_{n,m} \leq 1$ for $n \neq m$. To reduce dimensionality, we discard redundant elements (e.g., the lower triangle and diagonal) and vectorize the strictly upper triangular part of $\mathbf{q}$ to obtain a one-dimensional column vector $\mathbf{Q} \in \mathbb{R}^L$, where $L = N(N-1)/2$. Order parameter estimation and its temporal evolution were performed using the full dataset, excluding

those containing spurious signals (event where spectra captures high intensity random signals).

S3 Applicability of the Order Parameter in a Dynamic System

While the concept of an order parameter is traditionally associated with systems in equilibrium, a natural question arises regarding its applicability to spectral diffusion, where fluctuations in the local environment can occur on timescales ranging from hundreds of ns to ms. This concern requires justification.

In our experiments, spectral diffusion was measured with a temporal resolution of 500µs, which is the fastest timescale accessible in our setup due to photon count statistics and acquisition constraints. For analysis, we used a moving window of size 10, corresponding to a duration of 5ms. This choice is motivated by the observation that significant temporal correlations persist on this timescale, as shown in Fig. 4b of the main manuscript, where the autocorrelation function remains nonzero for up to about 50 lags (i.e., 25ms).

Although faster µs-scale dynamics may exist, they are averaged within each 5ms bin. Therefore, it is reasonable to assume local quasi-stationary behavior over such windows, permitting the application of the order parameter as described in Section S2. In addition, replica theory has been widely used in studying broad range of probelms such as spin glass [6, 7] and random lasing[8].

S4 Relative stability in quantum emitters ZPL

To quantify the *relative stability* of a quantum emitter, we analyze the temporal evolution of the order parameter $|q|$, as shown in Fig. 3(b,c). For a perfectly stable overlap, $|q|$ should remain close to unity across all time windows, indicating a strong overlap with the reference spectrum and, therefore, a strong temporal correlation. In contrast, deviations from unity (that is, lower values of $|q|$) suggest instability. Importantly, we identify two complementary indicators of instability: (i) the *magnitude of deviation* from high $|q|$ values, and (ii) the *frequency of such deviations* over time. Even if the emitter occasionally returns to high overlap, frequent oscillations in $|q|$ reflect temporal inconsistency and therefore reduced stability. This is further substantiated in Fig. 4(c,d) by the power spectral density (PSD) analysis of the zero-phonon line (ZPL) trajectory: relatively unstable emitters exhibit a flatter PSD slope, often approaching values below 0.5, indicative of weaker temporal correlation. These quantifiers provide a robust framework for *pre-select emitters* with desirable stability characteristics prior to full-scale experiments.

References

[1] Senichev, A., Martin, Z.O., Peana, S., Sychev, D., Xu, X., Lagutchev, A.S., Boltasseva, A., Shalaev, V.M.: Room-temperature single-photon emitters in silicon nitride. Science Advances **7**(50), 0627 (2021) https://doi.org/10.1126/sciadv.

abj0627

[2] Martin, Z.O., Senichev, A., Maan, P., Ozlu, M.G., Marinova, M., Shang, Z., Lagutchev, A., Boltasseva, A., Shalaev, V.M.: Single-photon emitters in pecvd-grown silicon nitride films: from material growth to photophysical properties. Nanophotonics **14**(11), 1783–1793 (2025) https://doi.org/10.1515/nanoph-2024-0506

[3] Akbari, H., Biswas, S., Jha, P.K., Wong, J., Vest, B., Atwater, H.A.: Lifetime-limited and tunable quantum light emission in h-bn via electric field modulation. Nano Letters **22**(19), 7798–7803 (2022) https://doi.org/10.1021/acs.nanolett.2c02163

[4] Machielse, B., Bogdanovic, S., Meesala, S., Gauthier, S., Burek, M.J., Joe, G., Chalupnik, M., Sohn, Y.I., Holzgrafe, J., Evans, R.E., Chia, C., Atikian, H., Bhaskar, M.K., Sukachev, D.D., Shao, L., Maity, S., Lukin, M.D., Lončar, M.: Quantum interference of electromechanically stabilized emitters in nanophotonic devices. Phys. Rev. X **9**, 031022 (2019) https://doi.org/10.1103/PhysRevX.9.031022

[5] Parisi, G.: Order parameter for spin-glasses. Phys. Rev. Lett. **50**, 1946–1948 (1983) https://doi.org/10.1103/PhysRevLett.50.1946

[6] Marsh, B.P., Kroeze, R.M., Ganguli, S., Gopalakrishnan, S., Keeling, J., Lev, B.L.: Entanglement and replica symmetry breaking in a driven-dissipative quantum spin glass. Phys. Rev. X **14**, 011026 (2024) https://doi.org/10.1103/PhysRevX.14.011026

[7] Dotsenko, V.: Introduction to the Replica Theory of Disordered Statistical Systems, pp. 46–53. Cambridge University Press, Cambridge (2000)

[8] Fruhling, C., Wang, K., Chowdhury, S., Xu, X., Simon, J., Kildishev, A., Dou, L., Meng, X., Boltasseva, A., Shalaev, V.M.: Coherent random lasing in subwavelength quasi-2d perovskites. Laser & Photonics Reviews **17**(4), 2200314 (2023) https://doi.org/10.1002/lpor.202200314